Carbohydrate Polymers 82 (2010) 83–91

Contents lists available at ScienceDirect

Carbohydrate Polymers

journal homepage: www.elsevier.com/locate/carbpol

# Nanocomposite of carboxymethyl cellulose and attapulgite as a novel pH-sensitive superabsorbent: Synthesis, characterization and properties

Wenbo Wang[a,b], Aiqin Wang[a,*]

[a] Center for Eco-material and Green Chemistry, Lanzhou Institute of Chemical Physics, Chinese Academy of Sciences, Lanzhou, 730000, PR China
[b] Graduate University of the Chinese Academy of Sciences, Beijing, 100049, PR China

ARTICLE INFO

*Article history:*
Received 20 February 2010
Received in revised form 4 April 2010
Accepted 13 April 2010
Available online 20 April 2010

*Keywords:*
Superabsorbent nanocomposite
Carboxymethyl cellulose
Attapulgite
pH-sensitive
Swelling

ABSTRACT

Grafting vinyl monomers onto natural polysaccharides and then compounding with inorganic nano-scale clays become a preferred method to derive superabsorbents because it afforded unique environmental and commercial advantages. In current work, a series of superabsorbent nanocomposites were prepared by radical solution polymerization of sodium carboxymethyl cellulose (CMC), partially neutralized acrylic acid (NaA) and attapulgite (APT) using ammonium persulfate (APS) as an initiator and *N,N′*-methylenebisacrylamide (MBA) as a crosslinker. Fourier transform infrared spectroscopy (FTIR) spectra proved that NaA was grafted onto CMC backbone and APT participated in polymerization. APT nanofibrils were retained in nanocomposite and uniformly dispersed in the CMC-*g*–PNaA matrix as shown by X-ray diffraction (XRD), transmission electron microscopy (TEM) and field emission scanning electron microscope (FESEM) analyses. The thermal stability and water absorption of the nanocomposites were improved due to the incorporation of APT. The water absorption and gel strength depends on the MBA concentration. The remarkable pH-sensitivity and time-dependent swelling behavior of the nanocomposite in aqueous solution of cetyltrimethylammonium bromide (CTAB) were observed and discussed.



## 1. Introduction

Nanocomposites of polymer with clays have recently attracted great interest in scientific research and industrial application because such materials showed unique hybrid properties superior to their individual components and cost-efficient characteristic (Liu, 2007; Pavlidou & Papaspyrides, 2008; Wang, Du, et al., 2009). Superabsorbents are moderately crosslinked hydrophilic polymer networks that can absorb and retain large quantities of aqueous fluids even under certain pressure. Because of the particular superiorities over traditional absorbents (e.g. sponge, cotton, wood pulp and colloidal silica, etc.), superabsorbents have been extensively applied in many fields such as hygienic products (Kosemund et al., 2009), agriculture (Doane & Doane, 2005; Liang, Yuan, Xi, & Zhou, 2009; Puoci et al., 2008) wastewater treatment (Kaşgöz & Durmus, 2008; Kaşgöz, Durmuş, & Kaşgöz, 2008; Wang, Zhang, & Wang, 2008) and drug-delivery systems (Sadeghi & Hosseinzadeh, 2008; Wang, Zhang & Wang, 2009), etc. However, there are limitations to such applications because most of superabsorbents used as disposable particles are based on fully petroleum-based polymers with high production cost and serious environment impact (Kiatkamjornwong, Mongkolsawat, & Sonsuk, 2002). So the new types of multi-component superabsorbents derived from the naturally available raw materials are desired, and the organic–inorganic nanocomposites of natural polysaccharides with inorganic clays undoubtedly become promising materials because they showed both excellent performance and environmental friendly characteristics (Ray & Bousmina, 2005).

Among numerous polysaccharides (Chen, Liu, Tan, & Jiang, 2009; Li, Zhang, & Wang, 2007; Pourjavadi, Hosseinzadeh, & Sadeghi, 2007; Teli & Waghmare, 2009; Wang & Wang, 2009; Wu & Liu, 2008; Zeng, Wu, & Kennedy, 2008), cellulose is the most potential one because it is the most abundant natural polymer with excellent biodegradability and biocompatibility. However, the poor solubility of cellulose in water and most organic solvents and the poor reactivity make it difficult to be directly modified to fabricate other useful materials. By contrast, the derivative modification of cellulose can overcome these drawbacks. Carboxymethyl cellulose (CMC) is a representative cellulose derivative with carboxymethyl groups ($-CH_2-COONa$) bonded to some of the hydroxyl groups on cellulose backbone. It can be easily synthesized by the alkali-catalyzed reaction of cellulose with chloroacetic acid and has been widely used as a thickening agent and stabilizing agent. The polar

* Corresponding author. Tel.: +86 931 4968118; fax: +86 931 8277088.
*E-mail addresses:* aqwang@lzb.ac.cn, aqwang@licp.cas.cn (A. Wang).

0144-8617/$ – see front matter © 2010 Elsevier Ltd. All rights reserved.
doi:10.1016/j.carbpol.2010.04.026

carboxyl groups render the cellulose soluble, chemically reactive and strongly hydrophilic, and so the application of CMC in superabsorbent fields becomes attractive and promising (Suo, Qian, Yao, & Zhang, 2007).

Attapulgite (APT) is a kind of hydrated octahedral layered magnesium aluminum silicate mineral with exchangeable cations in its framework channels and reactive –OH groups on its surface (Krekeler & Guggenheim, 2008). It is a type of natural fibrous silicate clay, consisting of two double chains of the pyroxene-type $(SiO_3)^{2-}$ like amphibole $(Si_4O_{11})^{6-}$ running parallel to the fibre axis (Xiang, Peng, & Chen, 2006). It is expected that the type and amount of hydrophilic groups, network structure and properties of superabsorbents could be improved by the composite of APT with CMC at nanometer scale.

Based on above background, the series of novel superabsorbent nanocomposites based on CMC and APT were synthesized by radical solution polymerization. The structure and morphologies of the nanocomposite were characterized by Fourier transform infrared spectroscopy (FTIR), X-ray diffraction (XRD), thermogravimetric analysis (TGA), transmission electron microscopy (TEM) and field emission scanning electron microscope (FESEM). The gel strength, pH-sensitivity and the swelling behaviors of the nanocomposite in distilled water and cationic surfactant solutions were also evaluated, systematically.

## 2. Experimental

### 2.1. Materials

Sodium carboxymethyl cellulose (CMC, CP, 300–800 mPa s (25 g/L, 25 °C)) was from Sinopharm Chemical Reagent Co., Ltd, China. Acrylic acid (AA, chemically pure, Shanghai Shanpu Chemical Factory, Shanghai, China) was distilled under reduced pressure before use. APT micro-powder (Xuyi Colloidal Co., Jiangsu, China) was milled and passed through a 320-mesh screen (46 μm) prior to use. Ammonium persulfate (APS, analytical grade, Xi'an Chemical Reagent Factory, China) and *N,N′*-methylenebisacrylamide (MBA, chemically pure, Shanghai Chemical Reagent Corp., China) was used as received. Cetyltrimethylammonium bromide (CTAB, Beijing Chemical Reagents Company, China) was used as purchased. All other reagents used were of analytical grade and all solutions were prepared with distilled water.

### 2.2. Preparation of CMC-g–PNaA/APT nanocomposites

CMC powder (1.03 g) was dissolved in 30 mL distilled water in a 250-mL four-necked flask equipped with a mechanical stirrer, a thermometer, a reflux condenser and a nitrogen line to form a transparent sticky solution. The solution was heated to 60 °C and purged with $N_2$ for 30 min to remove dissolved oxygen. Then, 5 mL of aqueous solution of initiator APS (0.072 g) was added under continuous stirring and kept at 60 °C for 10 min to generate radicals. A 7.2 g of AA was neutralized by 7.6 mL 8.8 mol/L NaOH solution and fully mixed with 18 mg crosslinker MBA and the calculated amount of APT powder (0 g for CMC-*g*–PNaA; 0.44 g for 5 wt%; 0.95 g for 10 wt%; 2.08 g for 20 wt%; 2.78 g for 25 wt%) under magnetic stirring. After cooling the reactants to 50 °C, the mixture was added to the flask. The temperature was risen to 70 °C and maintained for 3 h to complete reaction. A nitrogen atmosphere was maintained throughout the reaction period. The obtained gel products were washed with distilled water for several times and dried to constant weight at 70 °C. Finally, the dried nanocomposites were ground and sieved to 40–80 mesh (180–380 μm).

### 2.3. Measurements of equilibrium water absorption and swelling kinetics

0.05 g of dry superabsorbent particle (180–380 μm) was soaked in excessive aqueous solutions at room temperature for 4 h to reach swelling equilibrium. The swollen superabsorbents were filtered using a 100-mesh sieve and drained for 20 min until no free water remained. After weighing the swollen superabsorbents, the equilibrium water absorption can be calculated using Eq. (1).

$$Q_{eq} = \frac{w_2 - w_1}{w_1} \quad (1)$$

$Q_{eq}$ is the equilibrium water absorption defined as grams of water per gram of sample; $w_1$ and $w_2$ are the mass of sample before and after swelling, respectively.

Swelling kinetics of superabsorbents in distilled water and CTAB solution was measured as follows: 0.05 g of superabsorbent was placed in 500 mL beaker and then 200 mL of aqueous solution was added. The swollen gel was filtered by a sieve after a set interval and the water absorption at a given swelling time was derived from the mass changes before and after swelling. In all cases three parallel samples were used and the averages were reported in this paper.

### 2.4. Evaluation of pH-sensitivity

The buffer solutions of various pHs were prepared by combining $KH_2PO_4$, $K_2HPO_4$, $H_3PO_4$, NaCl and NaOH solution properly. Ionic strengths of all the buffer solutions were adjusted to 0.1 M with NaCl solution. The pH values were determined by a pH meter (DELTA-320). The equilibrium water absorption ($Q_{eq}$) in each buffer solution was determined by a method similar to that in distilled water. The pH reversibility of the nanocomposite was investigated in terms of its swelling and deswelling in pH 7.2 and 2.0 buffer solutions of phosphate, respectively. Typically, the nanocomposite particle (about 0.05 g, 180–380 μm) was placed in a 100-mesh screen (150 μm) and was adequately contacted with pH 2.0 buffer solution until an equilibrium was achieved. Then, the swollen nanocomposite was soaked in pH 7.2 buffer solution for set time intervals. Subsequently, the swollen nanocomposite was filtered, weighed and calculated its water absorption at the given moment according to the mass change of samples before and after swelling (Eq. (1)). The consecutive time interval is 15 min for each cycle, and the same procedure was repeated for five cycles. After every measurement, each solution was renewed.

### 2.5. Characterizations

FTIR spectra were recorded on a Nicolet NEXUS FTIR spectrometer in 4000–400 $cm^{-1}$ region using KBr pellets. XRD analysis was performed using an X-ray power diffractometer with Cu anode (PAN analytical Co. X'pert PRO), running at 40 kV and 30 mA. TGA measurements were carried out on a Perkin–Elmer TGA-7 thermogravimeric analyzer (Perkin–Elmer Cetus Instruments, Norwalk, CT), with a temperature range of 25–800 °C at a heating rate of 10 °C/min using dry nitrogen purge at a flow rate of 50 mL/min. TEM micrographs were obtained using a JEM-2010 high-resolution transmission electron microscope (JEOL, Tokyo, Japan) at an acceleration voltage of 200 kV, the sample was ultrasonically dispersed in ethanol before observation. FESEM observations were carried out using a JSM-6701F field emission scanning electron microscope (JEOL) after coating the sample with gold film. The gel strength of the swollen nanocomposites was determined with the Physica MCR 301 rheometer (Germany) at 25 °C according to a previously developed method (Ramazani-Harandi, Zohuriaan-Mehr, Yousefi, Ershad-Langroudi, & Kabiri, 2006). The tested samples

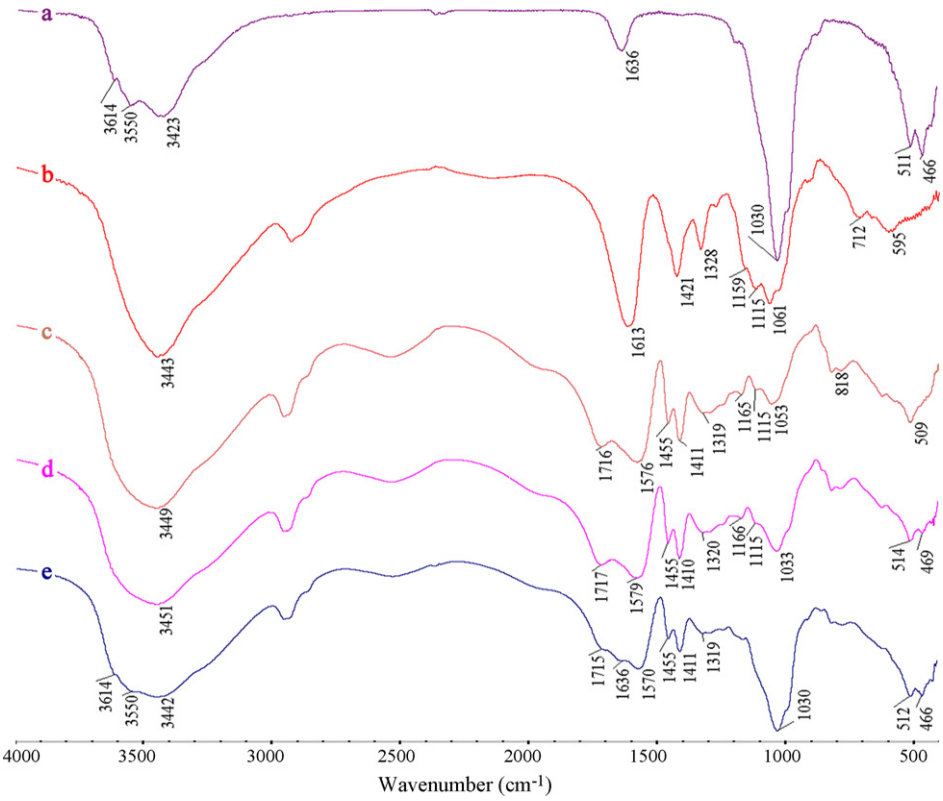


**Fig. 1.** FTIR spectra of (a) APT, (b) CMC, (c) CMC-*g*–PNaA, (d) CMC-*g*–PNaA/APT (10 wt%) and (e) the physical mixture of CMC-*g*–PNaA and APT.

were swollen in 0.9 wt% NaCl solution. The strain amplitude was chosen as 0.5% and the angular frequency $\omega$ was defined in the range of 0.1–100 rad/s. The results are the averages of at least three measurements.

## 3. Results and discussion

### 3.1. FTIR spectra

As shown in Fig. 1, the characteristic absorption bands of CMC at 1061, 1115 and 1159 $cm^{-1}$ (stretching vibrations of C–OH) were obviously weakened after reaction (Fig. 1(b–d)). The new bands at 1716–1717 $cm^{-1}$ (C = O stretching of –COOH) and 1576–1579 $cm^{-1}$ (asymmetric stretching of $-COO^-$ groups) and at 1455 and 1410 $cm^{-1}$ (symmetric stretching of $-COO^-$ groups) appeared in the spectra of CMC-*g*–PNaA and CMC-*g*–PNaA/APT (Fig. 1(c and d)). The position of these bands is close to that of PNaA, which revealed that NaA was grated onto CMC backbone. The asymmetric stretching vibration of –COONa groups on CMC at 1613 $cm^{-1}$ can be observed, which overlapped with the characteristic absorption of $-COO^-$ groups of grafted PNaA chains and formed a broad band. The $-COO^-$ bands of CMC-*g*–PNaA at 1576 $cm^{-1}$ shifted to 1579 $cm^{-1}$ after forming CMC-*g*–PNaA/APT, which implied the incorporation of APT decreased the hydrogel bonding interaction among polymer chains in contrast to CMC-*g*–PNaA. In addition, the (Al)O–H stretching vibration at 3614 $cm^{-1}$, the (Si)O–H stretching vibration of APT at 3550 $cm^{-1}$ and the –OH bending vibration at 1636 $cm^{-1}$ disappeared in the spectrum of nanocomposite (Fig. 1(a and d)). However, they can be clearly observed in the spectrum of the physical mixture of CMC-*g*–PNaA with APT (Fig. 1(e)). The absorption band of APT at 1030 $cm^{-1}$ (≡Si–O stretching vibration) appeared in the spectrum of CMC-*g*–PNaA/APT with a weakened intensity (Fig. 1(d)), but it was observed in the spectrum of the physical mixture of CMC-*g*–PNaA with APT with a considerable intensity (Fig. 1(e)). These informations indicate that APT participated in the graft copolymerization reaction through its active silanol groups (Li, Wang, & Chen, 2004).

### 3.2. X-ray diffraction analysis

X-ray diffraction patterns of APT and CMC-*g*–PNaA/APT (10 wt% and 25 wt%) were shown in Fig. 2(a). It was noticed that APT shows a strong reflection at $2\theta = 8.41^\circ$ with a basal spacing ($d$) of 1.051 nm. After compounding with CMC-*g*–PNaA, this reflection of APT can still be observed in the diffraction pattern of nanocomposite without obvious shift of peak position. This observation indicates that the crystalline structure of APT has not been destroyed during reaction, and the nano-scale APT fibril was retained and compounded with the CMC-*g*–PNaA matrix without intercalation. This result is consistent with the TEM and FESEM observations and confirmed the formation of nanocomposite.

### 3.3. Thermal analysis

The effect of introduced APT on the thermal stability of the nanocomposite was investigated using TGA technique and is shown in Fig. 2(b). It can be seen that the weight-loss rate of CMC-*g*–PNaA/APT is obviously slower than that of CMC-*g*–PNaA. At the initial stage, the weight loss about 21 wt% below 316 °C for CMC-*g*–PNaA, about 18 wt% below 317 °C, about 17 wt% below 317 °C and about 19 wt% below 318 °C for CMC-*g*–PNaA/APT (5, 10 and 20 wt%, respectively) was ascribed to the removal of water absorbed, the dehydration of saccharide rings and the breaking of C–O–C bonds in the chain of CMC (Yang, Li, He, Ren, & Wang, 2009). The minor weight loss about 17 wt% (316–431 °C) for CMC-*g*–PNaA, about 16 wt% (317–433 °C), about 14 wt% (317–436 °C) and about 14 wt% (318–438 °C) for CMC-*g*–PNaA/APT (5, 10 and 20 wt%, respectively) can be attributed to the elimination of the water molecule from

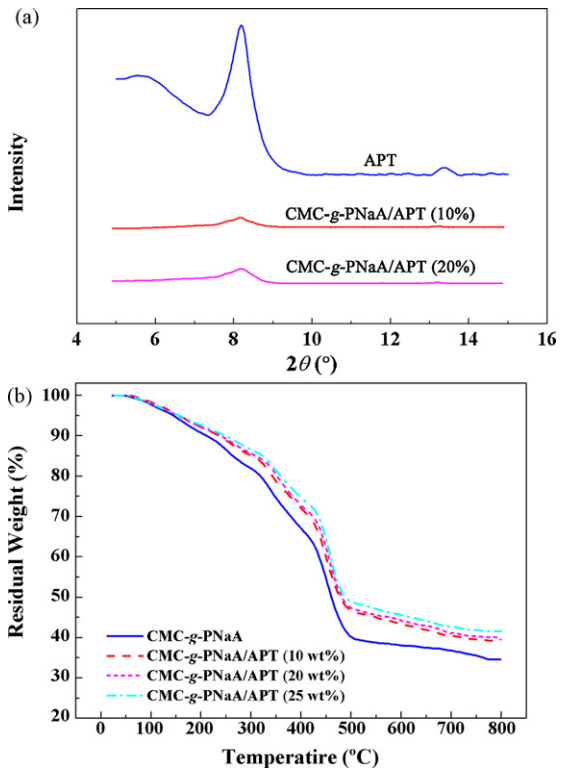


**Fig. 2.** (a) XRD patterns of APT and CMC-*g*–PNaA/APT nanocomposite with 10 wt% and 20 wt% of APT; (b) TGA curves of CMC-*g*–PNaA and CMC-*g*–PNaA/APT nanocomposites with 5 wt%, 10 wt% and 20 wt% of APT.

the two neighboring carboxylic groups of the polymer chains due to the formation of anhydride and main-chain scission (Huang, Lu, & Xiao, 2007). The weight losses about 23 wt% from 431 to 494 °C for CMC-*g*–PNaA and about 22 wt% from 433 to 498 °C, about 21 wt% from 436 to 501 °C, about 20 wt% from 438 to 504 °C for CMC-*g*–PNaA/APT (5, 10 and 20 wt%, respectively) are due to the breakage of PNaA chains and the destruction of crosslinked network structure. Compared with CMC-*g*–PNaA, CMC-*g*–PNaA/APT nanocomposites showed lower total weight loss, which indicate that the incorporation of APT into CMC-*g*–PNaA polymeric network enhanced its thermal stability.

### 3.4. TEM and FESEM analysis

Incorporation of APT not only affected the composition of superabsorbent, but also can affect its structure and morphology. Fig. 3 shows the TEM and FESEM micrographs of APT and CMC-*g*–PNaA/APT nanocomposite. It was shown that APT exhibits a randomly oriented nano-scale fibril with the diameter of a single fibril less than 100 nm and the length of a single fibril is about several hundred of nanometers (Fig. 3(a and c)). The nano-scale APT fibril was also observed in the TEM image and FESEM micrograph of the composite, which was almost embedded within the CMC-*g*–PNaA matrix (Fig. 3(b and d)). This observation indicates that the APT nanofibril was uniformly dispersed in the nanocomposite without agglomeration and formed a homogeneous composition.

### 3.5. pH-sensitivity

Fig. 4 shows the variation of the water absorption for CMC-*g*–PNaA/APT nanocomposites with pH of external buffer solution (0.1 M). It was noticed that the water absorption is low at acidic pH values ($\leq$4), but dramatically increases until a plateau was reached when the pH > 4. As an anionic polymer, the $-COO^-$ and –COOH functional groups in its structure can convert with each other. In acidic medium, $-COO^-$ converted to –COOH groups. The hydrogen-bonding interaction among –OH and –COOH groups was strengthened and the degree of physical crosslinking was increased. As a result, the water absorption was reduced. As pH increased to the basic conditions, numerous –COOH groups trans-

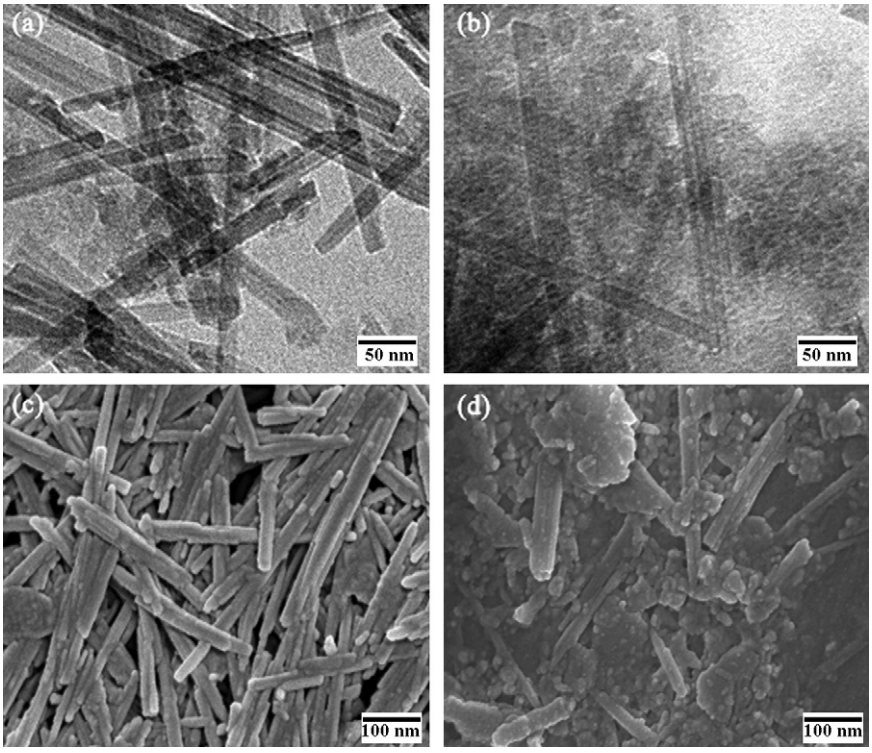


**Fig. 3.** TEM images of (a) APT and (b) CMC-*g*–PNaA/APT (10 wt%); FESEM micrographs of (c) APT and (d) CMC-*g*–PNaA/APT (10 wt%).

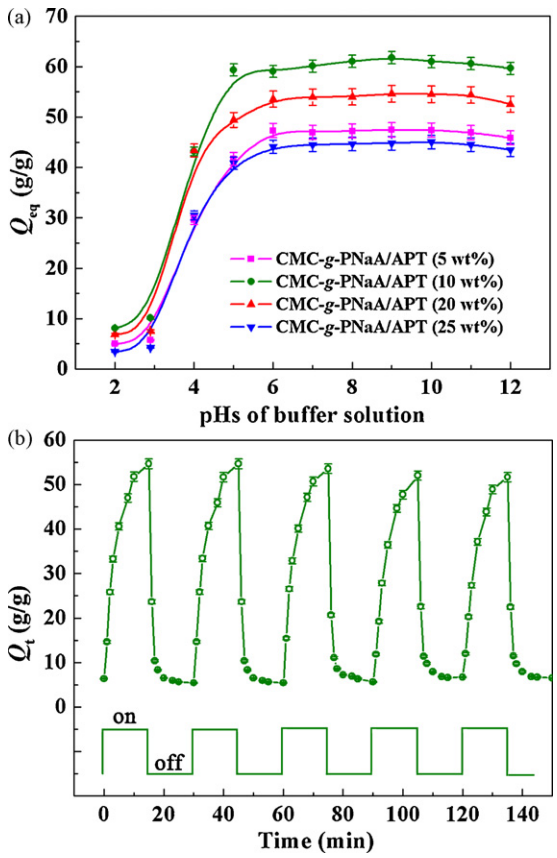


**Fig. 4.** (a) Variation of swelling ratio for CMC-*g*–PNaA/APT nanocomposites at the buffer solution with various pHs; (b) on–off switching behavior as reversible pulsatile swelling (pH 7.2) and deswelling (pH 2.0) of CMC-*g*–PNaA/APT (10 wt%) nanocomposite. The time interval between pH changes is 15 min.

form into $-COO^-$ groups and the hydrogen-bonding interaction was broken. Also, the electrostatic repulsion among polymer chains was increased due to the rapid increase in the number of negatively charged $-COO^-$ groups. Under this condition, the polymer network tends to swell more. For evaluating the pH reversibility of the nanocomposite, the swelling–deswelling behavior was determined in 0.1 M buffer solution of phosphate between pH 2 and 7.2 (Fig. 4(b)). The nanocomposite reached higher swelling ratio at pH 7.2, but the swollen gel rapidly shrinks due to the protonation of $-COO^-$ groups and exhibited intriguing on–off switching behavior. After five swelling–deswelling cycles, the nanocomposite still have better responsivity and reversibility, which makes them suitable candidates for controlled drug-delivery systems. The evident change of water absorption with altering the pH of external buffer solution confirmed the excellent pH-sensitive characteristic of CMC-*g*–PNaA/APT nanocomposites.

### 3.6. *Effects of crosslinker concentration on water absorption and gel strength*

Crosslinker concentration has usually greater influence on the water absorption of nanocomposite than others. As shown in Fig. 5(a), the water absorption rapidly decreased with increasing the concentration of crosslinker MBA from 2.69 to 10.78 mmol/L. According to Flory's theory (Flory, 1953), the increase of MBA concentration led to the increase of crosslinking density and the diminishment of network voids for holding water. This directly induces the rapid shrinkage of water absorption. The relationship between equilibrium water absorption and MBA concentration can be expressed by Eq. (2) and its logarithmic form (Eq. (3)) (Kabiri, Omidian, Hashemi, & Zohuriaan-Mehr, 2003).

$$Q_{eq} = kC_{MBA}^{(-n)} \tag{2}$$

$$ln(Q_{eq}) = \ln k + n \ln \frac{1}{C_{MBA}} \tag{3}$$

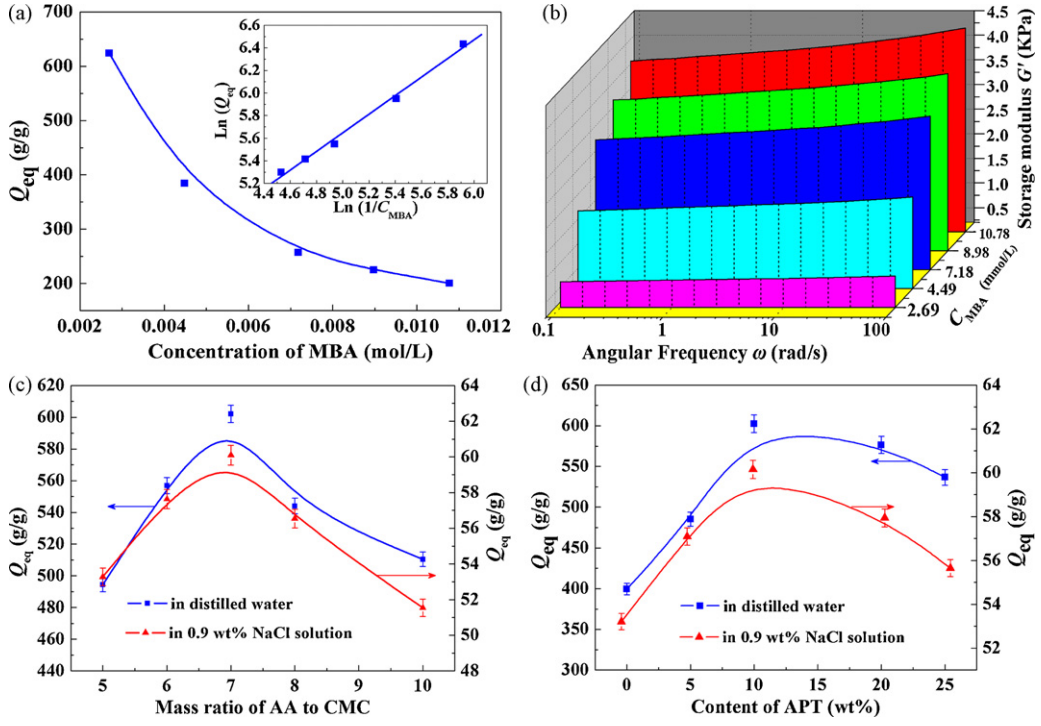


**Fig. 5.** (a) Effect of MBA concentration on the water absorption. The illustration is the plot of $\ln(Q_{eq})$ versus $\ln(1/C_{MBA})$; (b) angular frequency ($\omega$) dependence of the storage modulus ($G'$) at a constant strain (0.5%) for the nanocomposites with various crosslinking degrees; (c) effect of the mass ratio of AA to CMC on water absorption; and (d) effect of APT content on the water absorption.

$C_{MBA}$ is the concentration of crosslinker MBA; $k$ and $n$ are law constant for an individual superabsorbent. The plot of $\ln(Q_{eq})$ against $\ln(1/C_{MBA})$ gives perfect straight line with better linear correlation coefficient ($R^2 = 0.9967$). By fitting the experimental data, the $k$ and $n$ values can be calculated through the slope and intercept of the straight line. For CMC-*g*–PNaA/APT (10 wt%) nanocomposite, the relation of MBA concentration to equilibrium water absorption in distilled water follows the equation $Q_{eq} = 4.61C_{MBA}^{(-0.8240)}$.

The gel strength of the CMC-*g*–PNaA/APT nanocomposite with various crosslinking degrees was determined by rheological method (strain $\gamma = 0.5\%$; angular frequency $\omega = 0.1$–$100$ rad/s) and is shown in Fig. 5(b). It was noticed that the storage modulus ($G'$) of the nanocomposite increased with increasing the concentration of crosslinker MBA. The maximum $G'$ of the nanocomposite reached 3670 Pa ($\gamma = 0.5\%$, $\omega = 0.1$ rad/s) and 4340 Pa ($\gamma = 0.5\%$, $\omega = 100$ rad/s) when the crosslinking concentration is 10.78 mmol/L, and the $G'$ also reached 724 Pa ($\gamma = 0.5\%$, $\omega = 0.1$ rad/s) and 839 Pa ($\gamma = 0.5\%$, $\omega = 100$ rad/s) even if the concentration of crosslinker is 2.69 mmol/L.

### 3.7. Effects of mass ratio of AA to CMC on water absorption

As shown in Fig. 5(c), the water absorption increased as enhancing the mass ratio of AA to CMC, reached a maximum at 7 and then decreased. Due to the definite concentration of APS, the number of free radicals derived from the decomposition of APS is invariable. Thus, the concentration of monomers may directly affect the reaction rate and the amount of hydrophilic groups in polymer network. When the mass ratio of AA to CMC increased from 5 to 7, more monomers take part in graft polymerization reaction in the vicinity of active sites of CMC. As a result, the hydrophilicity of the polymeric network was improved due to the grafting of PNaA chains. Meanwhile, the osmotic pressure difference resulting from the dissociation of –COONa groups and the repulsive interaction among negative $–COO^-$ groups increased with increasing the dosage of AA, which contributes to enhance the water absorption. However, a high ratio of AA in the reaction system may increase the number of free radicals generated during the chain transfer reaction process and accelerate the polymerization rate. This increased the tangle of PNaA chains and the crosslinking density of polymeric network, and thus decreased the water absorption.

### 3.8. Effects of APT content on water absorption

Fig. 5(d) showed the swelling curves of equilibrium water absorption versus the content of APT. It was noticed that the water absorption increased with increasing APT content and reached a maximum at 10 wt%. APT is rigid and contains large amounts of active –OH groups on its surface, which can take part in the polymerization reaction as well as the construction of 3D network. As a result, the intertwining of polymeric chains was prevented and the hydrogen-bonding interaction between hydrophilic groups such as –COOH, $–COO^-$ and –OH, etc. was weakened. Thus, the degree of physical crosslinking decreased and the network voids for holding water regularly formed; this is extremely favorable to the improvement of water absorption.

It was also noticed from Fig. 5(d) that the water absorption decreased when APT content exceeded 10 wt%. According to previous report (Lin, Wu, Yang, & Pu, 2001), ultrafine clay powder may act as additional crosslinking points in polymer networks. The chemical composite of APT with polymeric matrix enhanced the crosslinking density of nanocomposite and minimized the network voids for absorbing and holding water. In addition, the excessive APT particles may physically stack in the network voids. On the one hand, some voids were plugged up and the water-holding capability decreased; on the other hand, the filling of excess APT decreased the ratio of hydrophilic groups in unit volume and the hydrophilicity of nanocomposite. Consequently, the water absorption decreased with the increase of APT content above 10 wt%. A similar tendency was also observed for poly(sodium acrylate)/sepiolite superabsorbent nanocomposite (Santiago, Mucientes, Osorio, & Poblete, 2006).

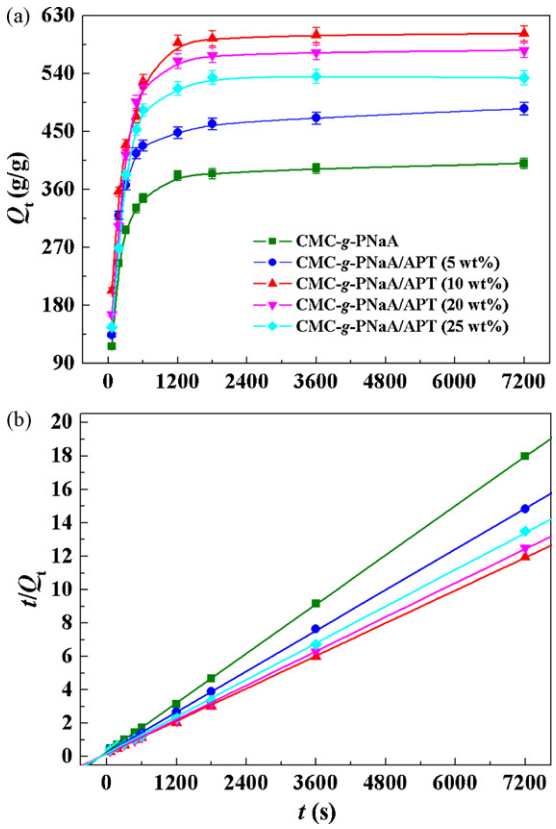


**Fig. 6.** Swelling kinetic curves of superabsorbents in distilled water (a) and $t/Q_t$ versus $t$ graphs of CMC-*g*–PNaA/APT (b).

### 3.9. Swelling kinetics in distilled water

Fig. 6 represented the swelling kinetic curves of the superabsorbents with various amounts of APT in distilled water. It can be seen that the swelling rate of the nanocomposites is faster within 1200 s and then reached a plateau. In this section, the swelling kinetics can be expressed by Schott's pseudo second order kinetics model (Eq. (4)) (Schott, 1992).

$$\frac{t}{Q_t} = \frac{1}{K_{is}} + \frac{1}{Q_\infty}t \tag{4}$$

$Q_t$ is the water absorption at a given swelling time $t$ (s); $Q_\infty$ (g/g) is the power parameter, denoting the theoretical equilibrium water absorption; $K_{is}$ is the initial swelling rate constant (g/g s). As shown in Fig. 6(b), the plots of $t/Q_t$ versus $t$ exhibited a perfect straight line with good linear correlation coefficient, which indicates that the swelling behaviors of the nanocomposites follow the pseudo second order model. By fitting experimental data using Eq. (4), the values of $K_{is}$ and $Q_\infty$ can be calculated through the slope and intercept of the above lines. The $K_{is}$ values are 3.6062, 4.3358, 5.8834, 5.5469 and 5.0633 g/g s, and the $Q_\infty$ values are 407, 493, 614, 588 and 547 g/g for CMC-*g*–PNaA, CMC-*g*–PNaA/APT (5 wt%), CMC-*g*–PNaA/APT (10 wt%), CMC-*g*–PNaA/APT (15 wt%) and CMC-*g*–PNaA/APT (20 wt%), respectively. According to the obtained values of $K_{is}$ and $Q_\infty$ for each superabsorbents, it can be concluded that the swelling rate decreased as the order:

CMC-*g*–PNaA/APT (10 wt%) > CMC-*g*–PNaA/APT (15 wt%) > CMC-*g*–PNaA/APT (20 wt%) > CMC-*g*–PNaA/APT (5 wt%) > CMC-*g*–PNaA.

Obviously, the incorporation of APT improved the initial swelling rate. As is discussed above, moderate APT contents may improve the three-dimensional network structure of the nanocomposite because APT participates in the construction of network. The improvement of network structure is favorable to the diffusion of water molecules into the network and facilitates to the relaxation of polymer chains. As a result, the swelling rate of the superabsorbent could be improved by the introduction of rigid APT. For CMC-*g*–PNaA/APT (10, 15 and 20 wt%) nanocomposites, the further increased APT content (>10 wt%) may decrease the hydrophilicity of polymeric network and obstruct the network voids, and so the rapid diffusion of water molecules was restricted and the swelling rate was correspondingly decreased.

### 3.10. Effects of cationic surfactant on water absorption

Fig. 7 represents the swelling kinetic curves of CMC-*g*–PNaA/APT (10 wt%) nanocomposite in CTAB solution with various concen-

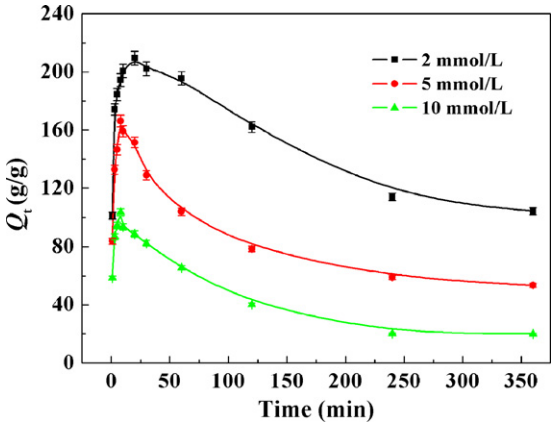


**Fig. 7.** Kinetic swelling curves of CMC-*g*–PNaA/APT (10 wt%) in 2, 5 and 10 mmol/L CTAB solutions.

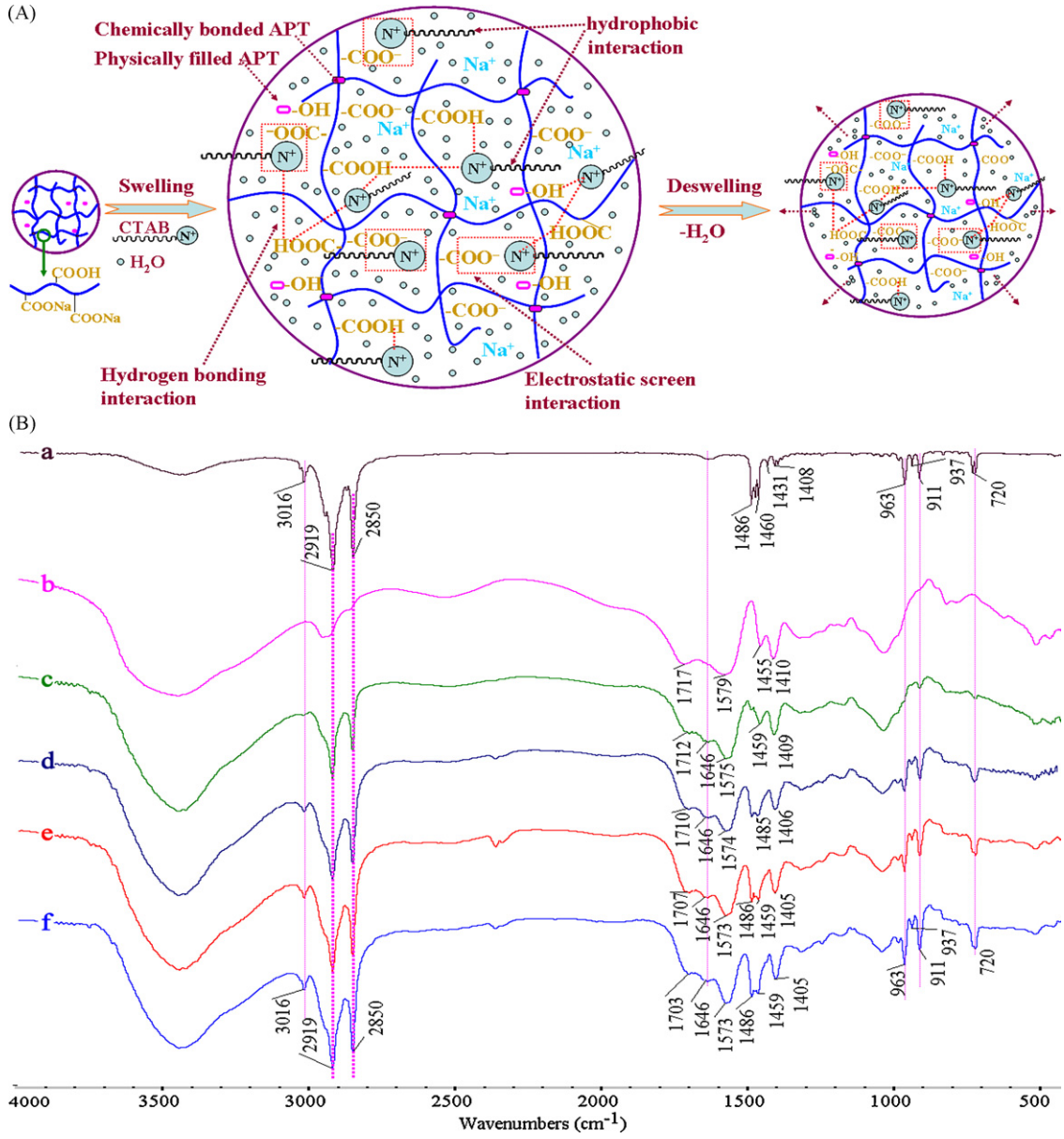


**Fig. 8.** (A) Proposed mechanism for the swelling–deswelling of the nanocomposite in CTAB solution; (B) FTIR spectra of (a) CTAB, (b) CMC-*g*–PNaA/APT (10 wt%) nanocomposite and the nanocomposite after swelling in 10 mmol/L CTAB solution for (c) 1 min, (d) 10 min, (e) 30 min and (f) 360 min.

trations. As can be seen, the water absorption rapidly increased with prolonging contact time during the first 600 s, reached a maximum and then decreased until swelling almost keeps a constant. The required time of reaching the maximum absorption for high concentration of CTAB is less than that for low concentration. This obvious time-dependent swelling behavior is known as overshooting effect (Díez-Peña, Quijada-Garrido, & Barrales-Rienda, 2003), and may be ascribed to the collaborative effect of three actions depicted in Fig. 8(A): (i) the electrostatic screen of positively charged amide cations to negatively charge $-COO^-$ groups; (ii) the hydrogen-bonding interactions among the –COOH groups on polymer chains and the quaternary ammonium cations; (iii) the hydrophobic interaction of long alkal chains in polymer network. On the one hand, the electrostatic interactions screened the negative charges of $-COO^-$ groups and weakened the repulsion among polymer chains; on the other hand, the ammonium groups formed hydrogen bonds with –COOH groups, which generated an additional physical crosslinking to make the network shrink. In addition, the entrance of CTAB with long alkyl chains into the polymer network decreased its hydrophilicity, which is also responsible for the deswelling of nanocomposite. FTIR spectra (Fig. 8(B)) showed the change of functional groups of CMC-*g*–PNaA/APT after swelling in 10 mmol/L CTAB solution for different time. The characteristic absorption bands of CTAB at 2919 $cm^{-1}$ (overlaps band of the C–H symmetric stretching of $-CH_3$ and the C–H asymmetric stretching of $-CH_2$), 2850 $cm^{-1}$ (C–H symmetric stretching of $-CH_2$), 1486 $cm^{-1}$ (H–C–H scissor bending of $-CH_2$), 1459 $cm^{-1}$ (H–C–H scissor bending of $-CH_3$), 963 $cm^{-1}$ (C–N stretching vibration), 911 $cm^{-1}$ (our-plane wagging of $-CH_2$) and 720 $cm^{-1}$ (in-plane deformations rocking of $-CH_2$) appeared in the spectra of nanocomposite after swelling in CTAB solution, and their intensity gradually increased with prolonging the contact time. This indicates that CTAB was entered into polymer network through a stringendo diffusion. Compared with the nanocomposite before swelling, the –COOH and $-COO^-$ absorption bands of the nanocomposite after swelling shifted from 1717 to 1703 $cm^{-1}$ (for –COOH) and from 1579 to 1573 $cm^{-1}$ (for $-COO^-$) with prolonging contact time, which implied the formation of strong hydrogen bonds in polymer network.

## 4. Conclusions

As a part of the efforts to reduce the excessive consumption of petroleum resources and the environmental impact resulting from industrial polymers, the superabsorbent nanocomposites were prepared from biopolymer CMC and naturally occurring nano-scale APT clay by free-radical solution polymerization. FTIR analysis confirmed that NaA monomers had been grafted onto CMC macromolecular chains and APT participated in the polymerization reaction by its active –OH groups. XRD, TEM and FESEM analyses revealed that the nano-scale APT crystalline fibrils have not been destroyed during polymerization, which led to a better dispersion in polymeric matrix and embedded within the matrix to form a nanocomposite. The incorporation of APT enhanced the swelling capability and rate of the nanocomposite, and the best water absorption was achieved at 10 wt% of APT. The nanocomposites deswell at acidic medium and swell at basic medium, and exhibited excellent pH-sensitive characteristics. The cyclic swelling–deswelling tests implied that the pH-sensitivity is reversible, and intriguing on–off switching swelling behaviors were observed. Besides pH-sensitivity, the time-dependent swelling behaviors of the nanocomposites were observed in the solution of cationic surfactant CTAB, and the required time of reaching maximum absorption was decided by the concentration of CTAB. Thus, superabsorbent nanocomposites based on renewable and biodegradable CMC and naturally occurring nano-scale APT showed excellent swelling capability, swelling rate, pH-sensitivity and intriguing time-dependent swelling characteristics, which can be used as potential water-manageable materials for various applications.

## Acknowledgements

The authors thank for jointly supporting by the National Natural Science Foundation of China (no. 20877077) and “863” Project of the Ministry of Science and Technology, PR China (no. 2006AA100215).

## References

Chen, Y., Liu, Y. F., Tan, H. M., & Jiang, J. X. (2009). Synthesis and characterization of a novel superabsorbent polymer of *N,O*-carboxymethyl chitosan graft copolymerized with vinyl monomers. *Carbohydrate Polymers*, *75*, 287–292.

Doane, S. W., & Doane, W. M. (2005). *Superabsorbent polymer product and use in agriculture*. US Pat. App.11/269,214.

Díez-Peña, E., Quijada-Garrido, I., & Barrales-Rienda, J. M. (2003). Analysis of the swelling dynamics of cross-linked P(N-iPAAm-*co*-MAA) copolymers and their homopolymers under acidic medium. A kinetics interpretation of the overshooting effect. *Macromolecules*, *36*, 2475–2483.

Flory, P. J. (1953). *Principles of polymer chemistry*. New York: Cornell University Press.

Huang, Y. H., Lu, J., & Xiao, C. B. (2007). Thermal and mechanical properties of cationic guar gum/poly(acrylic acid) hydrogel membranes. *Polymer Degradation and Stability*, *92*, 1072–1081.

Kabiri, K., Omidian, H., Hashemi, S. A., & Zohuriaan-Mehr, M. J. (2003). Synthesis of fast-swelling superabsorbent hydrogels: effect of crosslinker type and concentration on porosity and absorption rate. *European Polymer Journal*, *39*, 1341–1348.

Kaşgöz, H., & Durmus, A. (2008). Dye removal by a novel hydrogel-clay nanocomposite with enhanced swelling properties. *Polymers for Advanced Technologies*, *19*, 838–845.

Kaşgöz, H., Durmuş, A., & Kaşgöz, A. (2008). Enhanced swelling and adsorption properties of AAm-AMPSNa/clay hydrogel nanocomposites for heavy metal ion removal. *Polymers for Advanced Technologies*, *19*, 213–220.

Kiatkamjornwong, S., Mongkolsawat, K., & Sonsuk, M. (2002). Synthesis and property characterization of cassava starch grafted poly[acrylamide-*co*-(maleic acid)] superabsorbent *via* γ-irradiation. *Polymer*, *43*, 3915–3924.

Kosemund, K., Schlatter, H., Ochsenhirt, J. L., Krause, E. L., Marsman, D. S., & Erasala, G. N. (2009). Safety evaluation of superabsorbent baby diapers. *Regulatory Toxicology and Pharmacology*, *53*, 81–89.

Krekeler, M. P. S., & Guggenheim, S. (2008). Defects in microstructure in palygorskite–sepiolite minerals: A transmission electron microscopy (TEM) study. *Applied Clay Science*, *39*, 98–105.

Li, A., Wang, A. Q., & Chen, J. M. (2004). Studies on poly(acrylic acid)/attapulgite superabsorbent composite. I. Synthesis and characterization. *Journal of Applied Polymer Science*, *92*, 1596–1603.

Li, A., Zhang, J. P., & Wang, A. Q. (2007). Utilization of starch and clay for the preparation of superabsorbent composite. *Bioresource Technologies*, *98*, 327–333.

Liang, R., Yuan, H. B., Xi, G. X., & Zhou, Q. X. (2009). Synthesis of wheat straw-*g*-poly(acrylic acid) superabsorbent composites and release of urea from it. *Carbohydrate Polymers*, *77*, 181–187.

Lin, J. M., Wu, J. H., Yang, Z. F., & Pu, M. L. (2001). Synthesis and properties of poly(acrylic acid)/mica superabsorbent nanocomposite. *Macromolecular Rapid Communication*, *22*, 422–424.

Liu, P. (2007). Polymer modified clay minerals: A review. *Applied Clay Science*, *38*, 64–76.

Pavlidou, S., & Papaspyrides, C. D. (2008). A review on polymer-layered silicate nanocomposites. *Progress in Polymer Science*, *33*, 1119–1198.

Pourjavadi, A., Hosseinzadeh, H., & Sadeghi, M. (2007). Synthesis, characterization and swelling behavior of gelatin-*g*-poly(sodium acrylate)/kaolin superabsorbent hydrogel composites. *Journal of Composite Materials*, *41*, 2057–2069.

Puoci, F., Iemma, F., Spizzirri, U. G., Cirillo, G., Curcio, M., & Picci, N. (2008). Polymer in agriculture: A review. *American Journal of Agricultural and Biological Sciences*, *3*, 299–314.

Ramazani-Harandi, M. J., Zohuriaan-Mehr, M. J., Yousefi, A. A., Ershad-Langroudi, A., & Kabiri, K. (2006). Rheological determination of the swollen gel strength of superabsorbent polymer hydrogels. *Polymer Testing*, *25*, 470–474.

Ray, S. S., & Bousmina, M. (2005). Biodegradable polymers and their layered silicate nanocomposites: In greening the 21st century materials world. *Progress in Materials Science*, *50*, 962–1079.

Sadeghi, M., & Hosseinzadeh, H. J. (2008). Synthesis of starch-poly(sodium acrylate-*co*-acrylamide) superabsorbent hydrogel with salt and pH-responsiveness properties as a drug delivery system. *Journal of Bioactive and Compatible Polymers*, *23*, 381–404.

Santiago, F., Mucientes, A. E., Osorio, M., & Poblete, F. J. (2006). Synthesis and swelling behaviour of poly(sodium acrylate)/sepiolite superabsorbent composites and nanocomposites. *Polymer International*, *55*, 843–848.

Schott, H. (1992). Swelling kinetics of polymers. *Journal of Macromolecular Science B*, *31*, 1–9.

Suo, A. L., Qian, J. M., Yao, Y., & Zhang, W. G. (2007). Synthesis and properties of carboxymethyl cellulose-*graft*-poly(acrylic acid-*co*-acrylamide) as a novel cellulose-based superabsorbent. *Journal of Applied Polymer Science*, *103*, 1382–1388.

Teli, M. D., & Waghmare, N. G. (2009). Synthesis of superabsorbent from carbohydrate waste. *Carbohydrate Polymers*, *78*, 492–496.

Wang, L., Zhang, J. P., & Wang, A. Q. (2008). Removal of methylene blue from aqueous solution using chitosan-*g*-poly(acrylic acid)/montmorillonite superadsorbent nanocomposite. *Colloid Surface A*, *322*, 47–53.

Wang, Q., Zhang, J. P., & Wang, A. Q. (2009). Preparation and characterization of a novel pH-sensitive chitosan-*g*-poly(acrylic acid)/attapulgite/sodium alginate composite hydrogel bead for controlled release of diclofenac sodium. *Carbohydrate Polymers*, *78*, 731–737.

Wang, W. B., & Wang, A. Q. (2009). Preparation, characterization and properties of superabsorbent nanocomposites based on natural guar gum and modified rectorite. *Carbohydrate Polymers*, *77*, 891–897.

Wang, X. Y., Du, Y. M., Luo, J. W., Yang, J. H., Wang, W. P., & Kennedy, J. F. (2009). A novel biopolymer/rectorite nanocomposite with antimicrobial activity. *Carbohydrate Polymers*, *77*, 449–456.

Wu, L., & Liu, M. Z. (2008). Preparation and properties of chitosan-coated NPK compound fertilizer with controlled-release and water-retention. *Carbohydrate Polymer*, *72*, 240–247.

Xiang, Y. Q., Peng, Z. Q., & Chen, D. J. (2006). A new polymer/clay nano-composite hydrogel with improved response rate and tensile mechanical properties. *European Polymer Journal*, *42*, 2125–2132.

Yang, F., Li, G., He, Y. G., Ren, F. X., & Wang, G. X. (2009). Synthesis, characterization, and applied properties of carboxymethyl cellulose and polyacrylamide graft copolymer. *Carbohydrate Polymers*, *78*, 95–99.

Zeng, D. F., Wu, J. J., & Kennedy, J. F. (2008). Application of a chitosan flocculant to water treatment. *Carbohydrate Polymers*, *71*, 135–139.